DE GRUYTER OPEN

Int. J. of Applied Mechanics and Engineering, 2017, vol.22, No.4, pp.901-919
DOI: 10.1515/ijame-2017-0058

ON THE PARAMETERS OF GEOMETRIC CONSTRAINTS FOR CRACKED PLATES UNDER TENSION – THREE-DIMENSIONAL PROBLEMS

M. GRABA
Kielce University of Technology
Faculty of Mechatronics and Mechanical Engineering
Department of Manufacturing Engineering and Metrology
Al. 1000-lecia PP 7, 25-314 Kielce, POLAND
E-mail: mgraba@tu.kielce.pl

This paper provides a comparative analysis of selected parameters of the geometric constraints for cracked plates subjected to tension. The results of three-dimensional numerical calculations were used to assess the distribution of these parameters around the crack front and their changes along the crack front. The study also involved considering the influence of the external load on the averaged values of the parameters of the geometric constraints as well as the relationship between the material constants and the level of the geometric constraints contributing to the actual fracture toughness for certain geometries.

Key words: CC(T), DEN(T) and SEN(T) specimens, geometric constraints, stress triaxiality parameter, Q stresses, normal stresses, crack.

1. Introduction

Elastic-plastic problems of fracture mechanics are formulated using the HRR solution [1], [2] proposed in 1968. This approach has been commonly used to describe stress fields near the crack tip in elastic-plastic materials. Before 1993, only 2D problems were considered and the analysis was limited to the predominantly plane stress or plane strain conditions. Then, in 1993-1995, [3-5] suggested that the HRR solution could be generalized for three-dimensional cases by introducing the stress triaxiality parameter T_z. However, the method described by Guo [3-5], like the HRR solution [1,2], takes into account only the first term of the asymptotic expansion. In the years 2007-2009, some researchers [6-8], following the example of O'Dowd and Shih [9-10], suggested that the description of stress fields proposed by Guo Wanlin could be improved by taking into consideration the influence of all the other terms of the asymptotic expansion in the form of the parameter Q^* [6-8]. The parameters T_z and Q^* not only improve the theoretical description of stress fields and make it similar to the exact solution, i.e. one obtained with a finite element method (FEM), but they can also be used to assess the actual fracture toughness of various structural elements, providing that the appropriate fracture criterion is applied [6,11-13]. Using the fracture criteria presented in these papers, it is necessary to know the proper measures of in-plane constraints (e.g., the Q stresses defined by O'Dowd and Shiha [9-10]), and the out-of-plane constraints, which can be appropriately found in [14,15] and [7] respectively.

In the specialist literature, the parameters T_z and Q^* are known to be measures of the so-called geometric constraints, i.e., constraints of a material during the occurrence of plastic deformations under external loads [16]. These parameters are not the only parameters used as measures of constraints in the fracture criteria. In 1968, McClintok [17] proposed to use the ratio of the average normal stresses σ_m to the yield strength σ_0, designated by σ_m/σ_0, in the fracture criterion. A year later, Rice and Tracey [18] employed the ratio of the average stresses σ_m to the effective stresses σ_{eff}, calculated according to the Huber-Misses-Hencky (HMH) hypothesis, σ_m/σ_{eff}. Some researchers have considered the influence of

geometric constraints on the distribution of stresses for three-dimensional cases, analyzing the actual stresses responsible for the crack opening [19], or the differences between the actual description obtained through the FEM analysis and that obtained on the basis of the HRR solution for a case of plane strain [20, 21]. It is difficult to discuss all the parameters in one article. In fact, several articles can be devoted to one parameter, describing its origin and relationships with the material constants or geometries. The aim of this paper is to characterize the parameters for basic geometries, i.e., those typical of cracked plates subjected to tension (Fig.1) using the following specimens: a center-cracked specimen under tension (CC(T)), a single-edge notched specimen under tension (SEN(T)) and a double-edge notched specimen under tension (DEN(T)). According to the FITNET procedures [22], these geometries are used to idealize complex structural elements. The knowledge of the values of these parameters as well as their relationships with the specimen geometry or the material characteristics can be useful to solve engineering problems in the area of fracture mechanics in order to estimate the stress distributions and assess the actual fracture toughness.

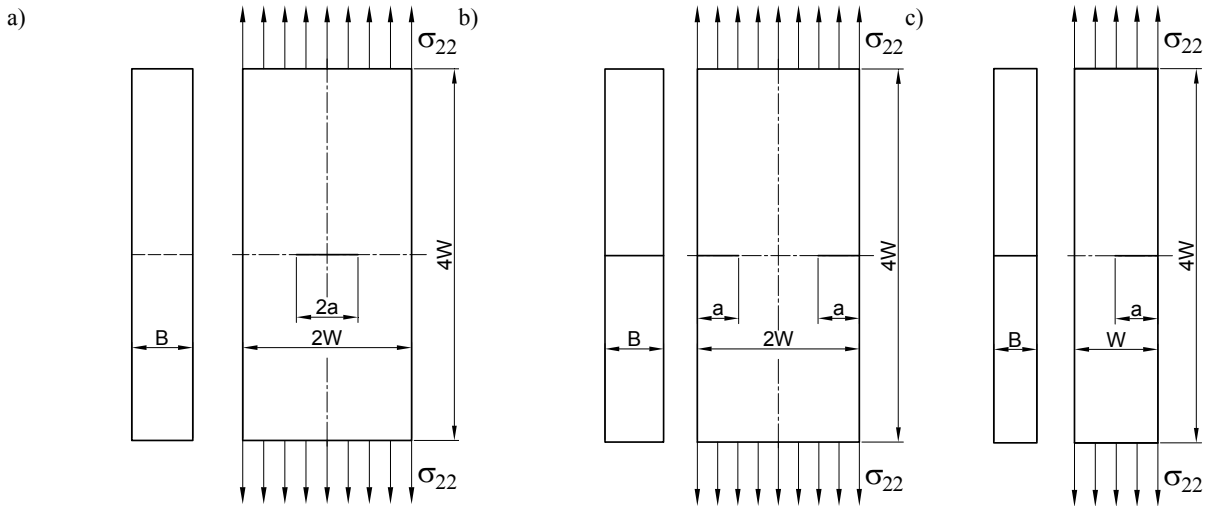

Fig.1. Geometries of the cracked specimens under tension: a) CC(T); b) DEN(T); c) SEN(T) specimens.

2. Defining selected parameters of the geometric constraints – 3D problems

The parameters of the geometric constraints for three-dimensional problems were briefly discussed in the Introduction; the dates of their use were also mentioned. In the literature on the elastic-plastic fracture mechanics we can find expressions defining the measures of the geometric constraints for three-dimensional cases:

- the ratio of the average normal stresses σ_m to the yield strength $\sigma_0 - \sigma_m/\sigma_{0:}$

$$\frac{\sigma_m}{\sigma_0} = \frac{1}{\sigma_0} \cdot \frac{\left(\sigma_{11} + \sigma_{22} + \sigma_{33}\right)}{3} \tag{2.1}$$

where σ_{11}, σ_{22}, and σ_{33} designate the normal constituents of the stress tensor;

- the ratio of the effective stresses σ_{eff} calculated according to the HMH hypothesis to the yield strength – σ_{eff}/σ_0 [17];
- the ratio of the average normal stresses σ_m to the effective stresses σ_{eff} according to the HMH hypothesis – σ_m/σ_{eff} [18];
- the stress triaxiality coefficient T_z [3-5], calculated as

$$T_z = \frac{\sigma_{33}}{(\sigma_{11} + \sigma_{22})} \tag{2.2}$$

- the parameter Q^* defined in [6-8]

$$Q^* = \frac{\sigma_{22\_FEM} - \sigma_{22\_GUO}}{\sigma_0} \tag{2.3}$$

where σ_{22_FEM} are the stresses responsible for the crack opening determined through the FEM analysis, and σ_{22_GUO} are the stresses responsible for the crack opening determined according to the solution proposed by Guo [3-5]

$$\sigma_{ij} = \sigma_0 \cdot \left(\frac{J_{far}}{\alpha \cdot \sigma_0 \cdot \epsilon_0 \cdot I_n(n, T_z) \cdot r} \right)^{\frac{1}{1+n}} \cdot \widetilde{\sigma_{ij}}(\theta, n, T_z), \tag{2.4}$$

while J_{far} is the J-integral calculated numerically around the far-field contour [7], $\varepsilon_0=\sigma_0/E$, E is Young's modulus, n is the exponent in the Ramberg-Osgood law, r and θ are polar coordinates defining the location of the point in the area around the crack tip, $I_n(n, T_z)$ and $\widetilde{\sigma_{ij}}(\theta, n, T_z)$ are functions determined from the algorithm presented in [3-5] and [7];

- the parameter Q^{pso} is the difference between the actual distribution of stresses σ_{22_FEM} and the estimated distribution of stresses for the predominantly plane strain conditions σ_{22_pso} normalized by the yield strength

$$Q^{pso} = \frac{\sigma_{22\_MES} - \sigma_{22\_pso}}{\sigma_0} \tag{2.5}$$

where

$$\sigma_{ij\_pso} = \sigma_0 \cdot \left(\frac{J}{\alpha \cdot \sigma_0 \cdot \epsilon_0 \cdot I_n(n, pso) \cdot r} \right)^{\frac{1}{1+n}} \cdot \widetilde{\sigma_{ij}}(\theta, n, pso) \tag{2.6}$$

while $I_n(n, pso)$ and $\widetilde{\sigma_{ij}}(\theta, n, pso)$ are the functions determined according to the algorithm presented in [1,2] and in [7] for a case of the predominantly plane strain conditions.

Among the parameters mentioned above, the parameters σ_m/σ_0, σ_m/σ_{eff} and T_z are considered to be stress triaxiality parameters related mainly to the thickness of the structural elements, while the parameters Q^* and Q^{pso} are measures of the geometric constraints largely dependent on the in-plane dimensions of the structural elements – the specimen width W and the crack length a.

It is necessary to know the parameters of the geometric constraints to use them. The literature does not provide values of the parameters – to determine them, we need to perform numerical calculations. There are no catalogues that help estimate the values of the parameters for any structure with a specified geometry and material characteristics. Reference [7] provides the approximation formulae to determine the values of the parameters T_m and Q^*_m, which are values of the parameters T_z and Q^* averaged across the thickness. The formulae are true for one geometry, i.e., the single-edge notched bending (SEN(B)) specimen, for which, under laboratory conditions, fracture toughness is determined. The use of the values of the parameters of the

geometric constraints averaged across the thickness is a good idea because the estimation of fracture toughness (or failure of a cracked structure based on failure assessment diagrams, FADs) is carried out for a specified thickness of a structural element and not for a specified cross-section.

3. Details of the numerical calculations

The selected parameters of the geometric constraints were analyzed for three 3D geometries under tension– the CC(T), SEN(T) and DEN(T) specimens – shown in Fig.1. The assumptions made for each specimen included the constant width $W=40mm$, the relative crack length $a/W=0.70$ and three thicknesses $B=\{2, 16, 40\}mm$. The assumption of the long crack ($a/W=0.70$) guarantees a high level of geometric constraints (high value of the Q stresses defined by O'Dowd [9, 10]. The use of three thicknesses allows us to analyze specimens whose stress state near the crack tip is similar to the predominantly plane stress conditions ($B=2mm$), the predominantly plane strain conditions ($B=40mm$) or the intermediate state ($B=16mm$).

The finite element analysis assumed an isotropic, uniform model of an elastic-plastic material, with the HMH plasticity condition in the form of formula (3.1)

$$\frac{\varepsilon}{\varepsilon_0}=\begin{cases}\sigma/\sigma_0 & \text{for} \quad \sigma\le\sigma_0 \\ \alpha\cdot\left(\sigma/\sigma_0\right)^n & \text{for} \quad \sigma>\sigma_0\end{cases} \tag{3.1}$$

where σ is the stress, ε is the strain, σ_0 is the yield strength, ε_0 is the deformation corresponding to the yield strength ($\varepsilon_0=\sigma_0/E$, where E is Young's modulus), α is the exponential constant in the Ramberg-Osgood (RO) law and n is the exponent in the RO law. In the calculations, it was assumed that the value of Young's modulus was constant $E=206$GPa, the value of the Poisson ratio was constant $\nu=0.3$ and the value of the exponential constant was $\alpha=1$. The default material for which the calculations were performed had the yield strength $\sigma_0=315$MPa and the strain hardening exponent $n=5$; the material was used by Sumpter and Forbes in their famous work dealing with the determination of fracture toughness [23].

All the numerical calculations were performed by means of ADINA SYSTEM 8.8 [24, 25]. The numerical models were created using the axes of symmetry existing in the specimens (by assuming appropriate boundary conditions); the crack tip was modeled as a quarter of an arc. The mesh was filled with eight-node finite elements (of the 3-D SOLID type). The authors of the ADINA program recommend that this type of elements be used to solve problems for specimens under tension. The author of this paper conducted a test to assess the mesh accuracy, which involved filling it with twenty-node 3-D SOLID type finite elements to confirm that the model was similar to the model with eight-node finite elements. The results obtained for the two meshes were similar. The external load was applied to the appropriate edge of the specimen using the displacement increasing in time. Table 1 provides details of the numerical models used to prepare this paper.

Figure 2 shows a sample numerical model used to analyze the SEN(T) specimen. The same method of modeling of the crack tip was employed for all the three specimens, CC(T), DEN(T) and SEN(T). The model was divided into finite elements. The other specimens were modeled in the same way to obtain easy-to-compare results.

The J-integral required for the analysis of the parameters of the geometric constraints was determined by means of the 'virtual shift method', which uses a virtual increase in the crack length. The J-integral was calculated for each layer across the specimen thickness; it was also averaged across the specimen thickness.

Table 1. Details of the numerical models of the cracked specimens under tension used in the 3D numerical analysis.

specimen type	**CC(T)**	**DEN(T)**	**SEN(T)**
number of axes of symmetry used	3		2
modeling (entire specimen, half, quarter)	an eighth of the specimen		a quarter of the specimen
boundary conditions	take into account the symmetry; applied to three axes of symmetry – vertical, horizontal and that going at half a distance of the thickness		take into account the symmetry; applied to two axes of symmetry – horizontal and that going at half a distance of the thickness
Number of FEs in the FEM model	15552 ÷ 16988 ÷ 17988		(15552 ÷ 16991 ÷ 18010)
total number of nodes in the FEM model	18018 ÷ 19638 ÷ 20790		(69999 ÷ 76299 ÷ 80779)
number of nodes per 1 FE	8		(20)
number of integration points per 1 FE	8		(27)
type of FE for 3D	small deformations, small displacements, 3-D type FEs with a mixed order interpolation scheme		
method of modeling of the crack tip	a quarter of the arc r_w=(1÷5)μm		
division of the arc near the crack tip	12 ES		
size of the area near the crack tip	(2÷4)mm		
division of the area near the crack tip	(18÷50) ES		
size of the largest and smallest FE in the area near the crack tip	division into 18 FEs ES_{min} → 2.90613 ·10^{-5}m (i.e. 1/1376·W) ES_{max} → 4.15161 ·10^{-4}m (i.e. 1/96·W) ES_{max}/ES_{min} = 14 division into 36 FEs ES_{min} → 1.45306 ·10^{-6}m (i.e. 1/2752·W) ES_{max} → 2.0758 ·10^{-4}m (i.e. 1/192·W) ES_{max}/ES_{min} = 14 division into 50 FEs ES_{min} → 1.04621 ·10^{-5}m (i.e. 1/3823·W) ES_{max} → 1.49458 ·10^{-4}m (i.e. 1/267·W) ES_{max}/ES_{min} = 14		division into 18 FEs ES_{min} → 2.90613 ·10^{-5}m (i.e. 1/1376·W) ES_{max} → 4.15161 ·10^{-4}m (i.e. 1/96·W) ES_{max}/ES_{min} = 100 division into 36 FEs ES_{min} → 1.45306 ·10^{-6}m (i.e. 1/2752·W) ES_{max} → 2.0758 ·10^{-4}m (i.e. 1/192·W) ES_{max}/ES_{min} = 100 division into 50 FEs ES_{min} → 1.04621 ·10^{-5}m (i.e. 1/3823·W) ES_{max} → 1.49458 ·10^{-4}m (i.e. 1/267·W) ES_{max}/ES_{min} = 100
number of layers in the division across the thickness	9		
density of FEs in the division across the thickness	20 ÷ 100		
relative coordinates of the layers across the thickness (x/B=0.000 – specimen axis, x/B=0.500 – specimen edge)	x/B={0.000 ; 0.119 ; 0.222 ; 0.309 ; 0.379 ; 0.434 ; 0.472 ; 0.483 ; 0.494 ; 0.500} ÷ x/B={ 0.000 ; 0.124 ; 0.230 ; 0.319 ; 0.390 ; 0.444 ; 0.480 ; 0.496 ; 0.499 ; 0.500};		
external load	applied to the specimen edge in the form of a displacement; with the displacement of the point at which the force was applied as $v_{II}=f(t)$ – displacement linearly increasing in time		

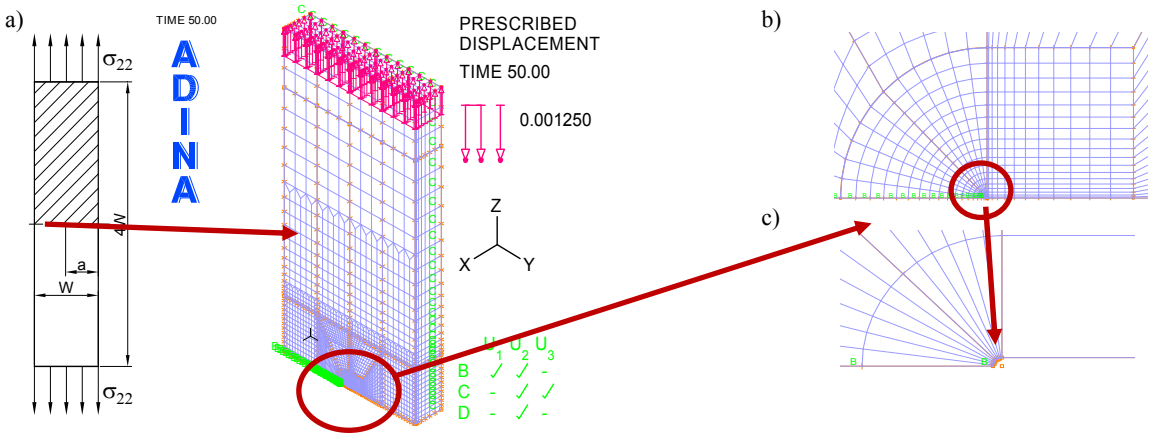

Fig.2. Numerical model of the SEN(T) specimen used in the numerical analysis: a) general model; b) magnified fragment of the mesh close to the crack tip; d) the crack tip model.

The parameters of the geometric constraints mentioned above were estimated for seven distances from the crack tip – $r=\{0.5, 1, 2, 3, 4, 5, 6\}\cdot J/\sigma_0$, separately for each layer across the specimen thickness. Since the maximum stresses responsible for the crack opening occur at a distance ranging $r=(0.5\div 2)\cdot J/\sigma_0$, with the assumption of large deformations, the analysis focused on determining the influence of the external load on the distribution of selected parameters of the geometric constraints for two measurement points near the crack tip – $r=1.0\cdot J/\sigma_0$ and $r=2.0\cdot J/\sigma_0$. The points were not selected at random; these distances were used by O'Dowd [9, 10] to determine the distribution of Q stresses, and these distances were considered to estimate the distribution of the values of the parameters T_z and Q^* in Ref. [7]. All the parameters of the geometric constraints were determined in the direction $\theta=0$; they were averaged using the following formula for the stress triaxiality parameter T_z

$$(T_z)_{av} = \frac{1}{B}\int_{-B/2}^{+B/2} T_z dx_3 . \tag{3.2}$$

The index '*av*' will designate the value averaged across the specimen thickness, B.

4. Analysis of the numerical calculation results

4.1. Stress triaxiality parameters σ_m/σ_0, σ_m/σ_{eff} and T_z

Figure 3 illustrates changes in the ratio of the average normal stresses to the yield strength (σ_m/σ_0), defined by formula (2.1). The further from the crack tip (the lower the value of r in the key to symbols), the lower the values of the average normal stresses. However, the closer to the edge ($x_3/B=0.5$), the larger the changes. The highest values of the average normal stresses are reported along the specimen axis ($x_3/B=0$). The closer to the crack tip, the greater the difference in the average normal stresses measured along the specimen axis and along its edge. It should be emphasized that the difference between the estimated stresses along the specimen axis ($x_3/B=0$) and those along its edge ($x_3/B=0.5$) decreases with an increasing distance from the crack tip. The analysis of the distribution of stresses around the crack front for the geometries considered in this paper shows that the highest values of the parameter σ_m/σ_0 are observed for the DEN(T) specimens, and the lowest for the CC(T) specimens; there are very small changes in the values of the parameter σ_m/σ_0 along the crack front for distances larger than $r=3.0\cdot J/\sigma_0$.

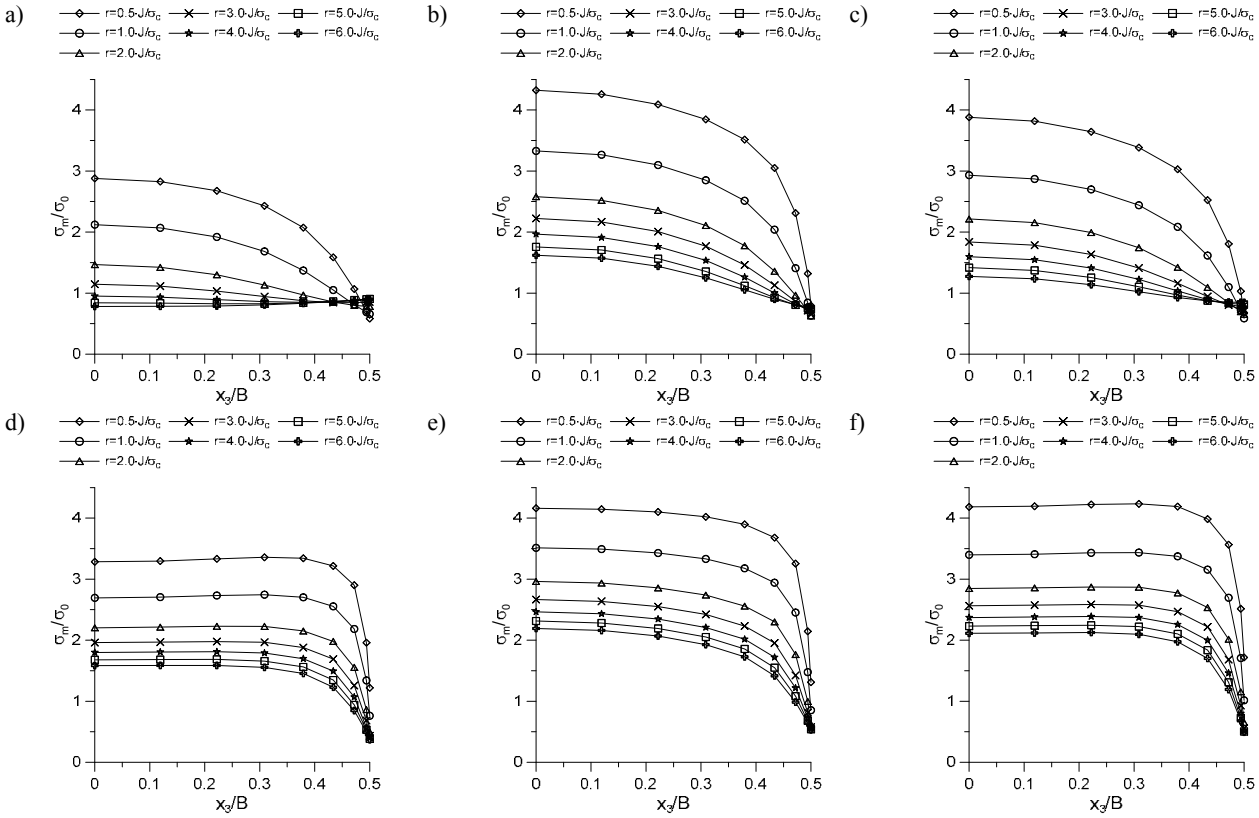

Fig.3. Distributions of the values of the parameter σ_m/σ_0 along the crack front for seven normalized distances for the specimens under tension at $a/W=0.70$, $W=40mm$, $n=5$, $\sigma_0=315$MPa, $P/P_0=1.20$: a) CC(T) $B=2mm$; b) DEN(T) $B=2mm$; c) SEN(T) $B=2mm$; d) CC(T) $B=40mm$; e) DEN(T) $B=40mm$; f) SEN(T) $B=40mm$.

The analysis of the results obtained for the specimens with the thickness $B/W=0.05$ shows that the values of the parameter σ_m/σ_0 along the edge decrease until $\sigma_m/\sigma_0=1$. For the specimens with a thickness satisfying the condition that $B/W=1$, the values of the parameter σ_m/σ_0 are almost constant along the crack front for certain distances assuming that the distance from the specimen axis is $x_3/B=0.38$. The closer to the specimen edge, the more rapid the changes in the values of the parameter σ_m/σ_0. It can be concluded that, along the specimen edge, the parameter σ_m/σ_0 decreases until $\sigma_m/\sigma_0=0.5$. All results are presented for external load P/P_0=1.20, where P_0 denoted limit load [26, 27].

Figure 4 shows changes in the values of the parameter σ_m/σ_{eff} for the specimens under tension with the thickness $B=16mm$ at external loads $P/P_0=1.20$. An increase in the distance from the crack tip causes a decreases in the value of the parameter σ_m/σ_{eff}. The larger the distance from the specimen axis ($x_3/B=0$) towards the edge ($x_3/B=0.50$), the lower the values of the parameter σ_m/σ_{eff}, which decrease until $\sigma_m/\sigma_{eff}=0.50$. For the CC(T) specimens, the values of the parameter σ_m/σ_{eff} around the crack tip ($r=0.5\cdot J/\sigma_0$) are smaller than those reported for the DEN(T) and SEN(T) specimens by the value of the yield strength.

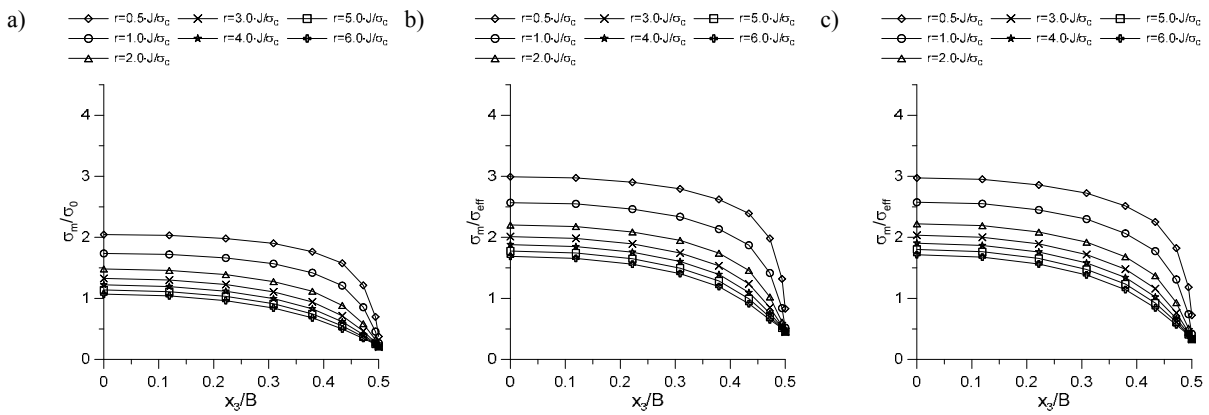

Fig.4. Distributions of the values of the parameter σ_m/σ_{eff} along the crack front for seven normalized distances for the specimens under tension at $a/W=0.70$, $W=40mm$, $n=5$, $\sigma_0=315$MPa, $P/P_0=1.20$: a) CC(T) $B=16mm$; b) DEN(T) $B=16mm$; c) SEN(T) $B=16mm$.

Figure 5 illustrates changes in the values of the parameter T_z – stress triaxiality coefficient – for an increase in the distance from the crack tip. The parameter T_z decreases with an increasing distance from the crack tip, but the highest values are observed for the cross-section along the specimen axis ($x_3/B=0$). The closer to the specimen edge, the smaller the values of the parameter T_z, which decrease until $T_z=0$. In the layers located along or close to the edge ($x_3/B=0.5$), the value of the parameter T_z is practically equal to zero when the distance is $r=1.0\cdot J/\sigma_0$ (or larger). In the case of specimens with the thickness $B/W=0.05$, the lowest values of the stress triaxiality coefficient T_z are observed for the CC(T) specimens, and the highest for the DEN(T) specimens. For thin specimens with $B/W=0.05$, we can see rapid changes along the crack front. For thick specimens with $B/W=1$, initially, the values of the parameter T_z are not affected by an increase in the distance from the specimen axis (the values of the parameter T_z along the crack front practically do not change), but when the cross-section is $x_3/B=0.43$, there are rapid changes and a decrease in the values of the parameter T_z.

Figure 6 compares the values of the parameters σ_m/σ_0, σ_m/σ_{eff} and T_z averaged across the thickness, designated by $(\sigma_m/\sigma_0)_{av}$, $(\sigma_m/\sigma_{eff})_{av}$ and $(T_z)_{av}$, respectively, for the three geometries considered in this paper. The analysis of the results indicates that the averaged values of the parameters $(\sigma_m/\sigma_0)_{av}$, $(\sigma_m/\sigma_{eff})_{av}$ and $(T_z)_{av}$ are the lowest for the CC(T) specimens, and the highest for the DEN(T) specimens. The conclusions are true for both analyzed distances from the crack tip, i.e., $r=1.0\cdot J/\sigma_0$ and $r=2.0\cdot J/\sigma_0$. It can be seen that when there is an increase in the external load (expressed by the value of the J-integral averaged across the thickness), the averaged values of the parameters $(\sigma_m/\sigma_0)_{av}$, $(\sigma_m/\sigma_{eff})_{av}$ and $(T_z)_{av}$ decrease nonlinearly reaching the predetermined values, which is true only for specimens with a relatively small thickness, $B/W<0.2$ (see Fig.7).

The three parameters discussed above - σ_m/σ_0, σ_m/σ_{eff} and T_z – known in the specialist literature as the stress triaxiality parameters, have values largely dependent on the thickness of the structural element, as shown in Figs 7a-c, where we can see changes in the values of the parameters averaged across the thickness (according to the procedure described by formula (3.2)) for the distance from the crack tip $r=2.0\cdot J/\sigma_0$. The use of the values of the parameters averaged across the thickness is fully justified because when fracture toughness is determined under laboratory conditions, the J-integral (or another measure) is determined for a specimen with a specified thickness. The values averaged across the thickness can be applied to formulate the fracture criteria.

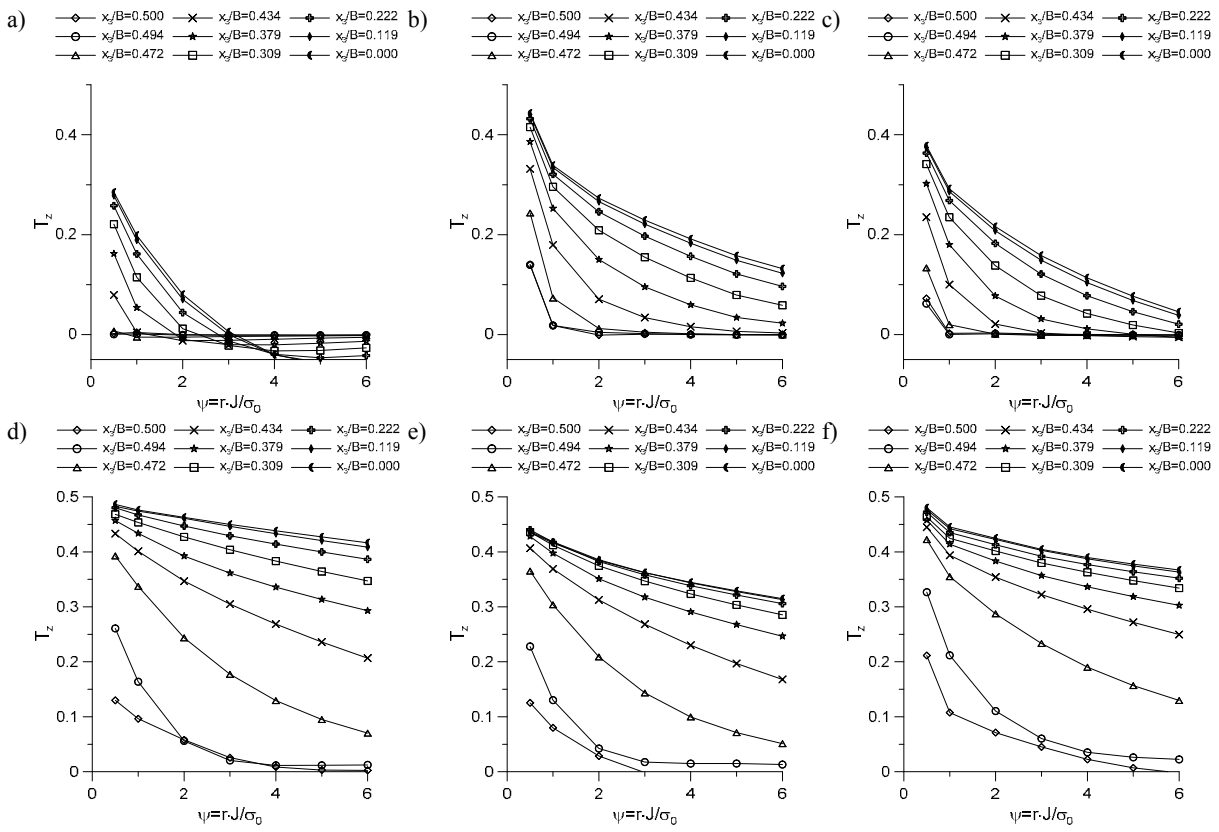

Fig.5. Distributions of the values of the parameter T_z near the crack tip for the particular layers across the thickness of the specimens under tension at $a/W=0.70$, $W=40mm$, $n=5$, $\sigma_0=315$MPa, $P/P_0=1.20$: a) CC(T) $B=2mm$; b) DEN(T) $B=2mm$; c) SEN(T) $B=2mm$; d) CC(T) $B=40mm$; e) DEN(T) $B=40mm$; f) SEN(T) $B=40mm$.

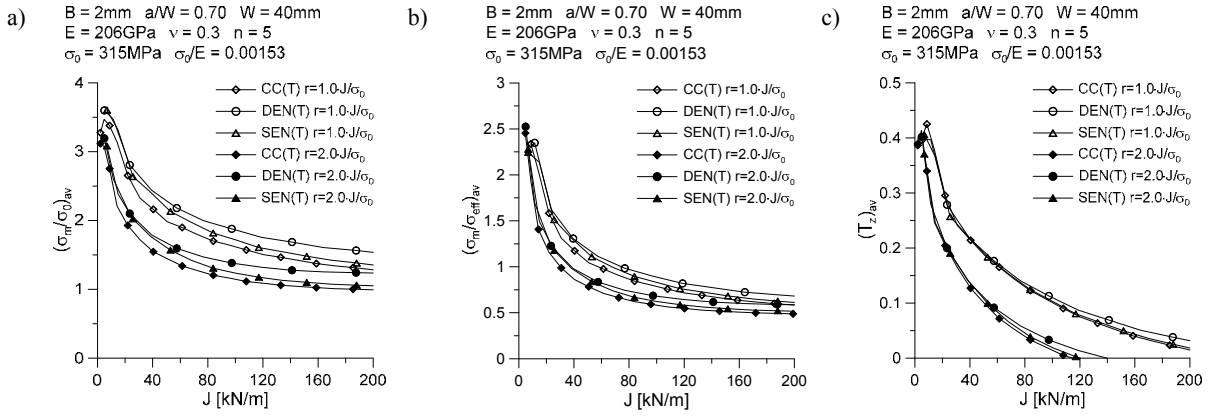

Fig.6. Comparison of the values of the parameters σ_m/σ_0 (a), σ_m/σ_{eff} (b) and T_z (c) averaged across the thickness of the CC(T), DEN(T) and SEN(T) specimens at $B=2mm$, $a/W=0.70$, $W=40mm$, $n=5$, $\sigma_0=315$MPa with the results reported for a whole spectrum of loads.

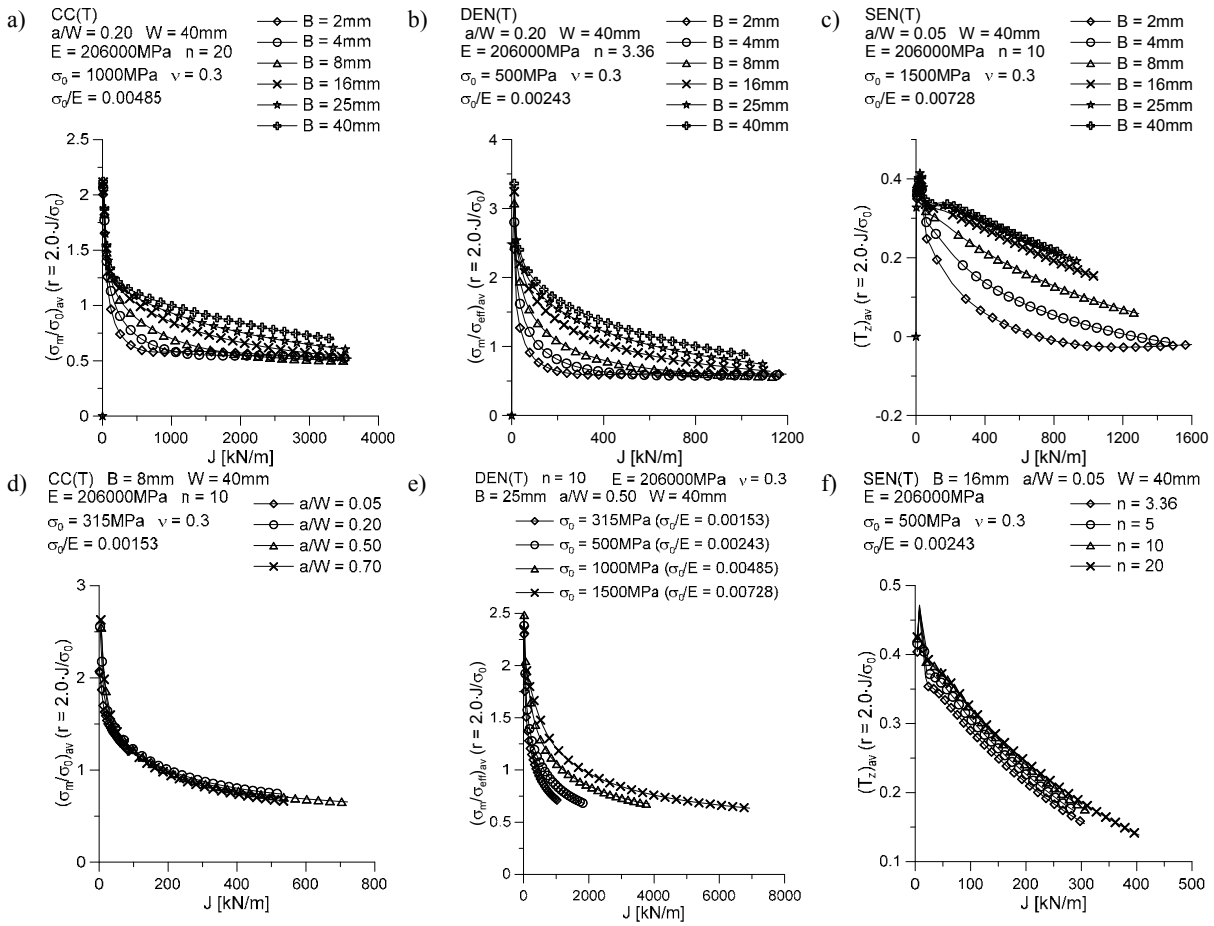

Fig.7. Influence of the specimen thickness, B, on the distribution of the parameters: a) $(\sigma_m/\sigma_0)_{av}$ for the CC(T) specimens; b) $(\sigma_m/\sigma_{eff})_{av}$ for the DEN(T) specimens; c) $(T_z)_{av}$ for the SEN(T) specimens; d) influence of the relative crack length, a/W, on the distribution of the parameter $(\sigma_m/\sigma_0)_{av}$, for the CC(T) specimens; e) influence of the yield strength, σ_0, on the distribution of the parameter $(\sigma_m/\sigma_{eff})_{av}$ for the DEN(T) specimens; f) influence of the strain hardening exponent in the RO law on the distribution of the parameter $(T_z)_{av}$ for the SEN(T) specimens.

The larger the thickness, the higher the values of the parameters $(\sigma_m/\sigma_0)_{av}$, $(\sigma_m/\sigma_{eff})_{av}$ and $(T_z)_{av}$ averaged across the thickness. It can be seen that the shapes of the curves $(\sigma_m/\sigma_0)_{av}=f(J)$, $(\sigma_m/\sigma_{eff})_{av}=f(J)$ and $(T_z)_{av}=f(J)$ change with increasing thickness. The analysis reveals that the crack length practically does not affect the values stress triaxiality parameters averaged across the thickness (Fig.7d). There is little dependence of the parameters $(\sigma_m/\sigma_0)_{av}$, $(\sigma_m/\sigma_{eff})_{av}$ and $(T_z)_{av}$ on the strain hardening exponent n in the RO law (see Fig.7f); this finding was used in the study presented in [7] for a simplified description of the distributions of the parameter $(T_z)_{av}$ for the SEN(B) specimens, by providing appropriate approximation formulae. The higher the degree of hardening, the lower the average value of the parameter T_z. It should be noted that the difference between two extreme curves for a material undergoing considerable strain hardening ($n=3.36$) and a material exhibiting poor strain hardening ($n=20$) for the same load does not exceed *15*%. As shown in Fig.7e, the yield strength has a substantial influence on the averaged values of the parameters $(\sigma_m/\sigma_0)_{av}$, $(\sigma_m/\sigma_{eff})_{av}$ and $(T_z)_{av}$. The higher the yield strength, the higher the values of the parameters $(\sigma_m/\sigma_0)_{av}$, $(\sigma_m/\sigma_{eff})_{av}$ and $(T_z)_{av}$ averaged across the thickness.

4.2. Parameters Q^* and Q^{pso} as measures of the in-plane constraints for 3D geometries

The measures of the geometric constraints, which are measures of the resistance of the material to the formation of plastic deformations, include the two parameters mentioned in the first section of this paper – Q^* and Q^{pso} – defined by formulae (2.3) and (2.5), respectively.

The parameter Q^* was first presented in [6-8]; it defines the difference between the numerical solution, which is considered to be the exact solution, and the theoretical solution proposed by Guo [3-5]. The use of the parameter Q^* to analyze stresses or assess fracture toughness requires knowledge of their distribution around the crack tip, apart from the distribution estimated numerically using the FEM analysis, as well as the knowledge of the stress triaxiality parameter T_z, being the basis of the solution proposed by Guo [3-5]. The parameter Q^* is regarded to be a measure of the constraints resulting from the in-plane dimensions of structural elements (specimen width and crack length) as well as those resulting from the thickness and the material characteristics.

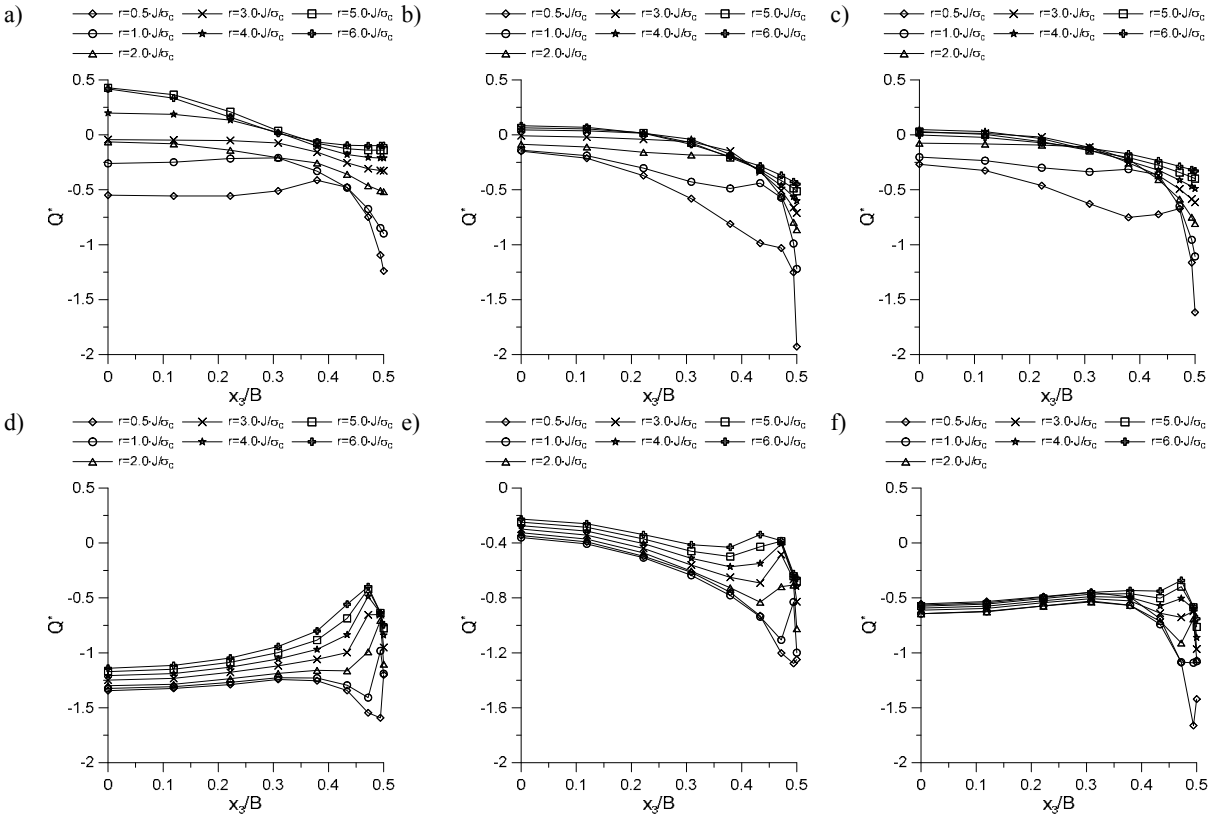

Fig.8. Distributions of the values of the parameter Q^* along the crack front for seven normalized distances obtained for the specimens under tension at $a/W=0.70$, $W=40mm$, $n=5$, $\sigma_0=315$MPa, $P/P_0=1.20$: a) CC(T) $B=2mm$; b) DEN(T) $B=2mm$; c) SEN(T) $B=2mm$; d) CC(T) $B=40mm$; e) DEN(T) $B=40mm$; f) SEN(T) $B=40mm$.

Figure 8 illustrates changes in the values of the parameter Q^* along the crack front for the analyzed CC(T), DEN(T) and SEN(T) specimens with the thickness being $B=2mm$ (Figs 8a-c) and $B=40mm$ (Figs 8d-f). The closer to the crack tip, the lower the value of the parameter Q^*; thus, we can assume a low level of geometric constraints near the crack tip. As can be seen, the distribution of the parameter Q^* along the crack front depends on the type of geometry, the thickness of the specimen and the distance from the crack tip. It is difficult to precisely determine the nature of the changes in the values of the parameter; actually, each case should be considered separately, and the analysis can be simplified when the value of the parameter Q^* averaged across the thickness (Q^*_{av}) is used.

The lowest level of constraints was reported for the CC(T) specimen, which coincided with the lowest value of the parameter Q^* (Fig.8d). By contrast, the DEN(T) specimen has a relatively high level of geometric constraints (Fig.8e). It should be emphasized, however, that the conclusions were drawn for one case of the geometry and material configurations; more details will be known after an analysis of the values averaged across the specimen thickness is completed.

Another parameter similar to the parameter Q^* is the parameter Q^{pso}, which determines the level of constraints resulting from the in-plane dimensions of the structural elements, defined by formula (2.5). This parameter is not frequently used to analyze problems related to fracture mechanics. It was described in [20, 21], where the authors tried to determine the difference between the distribution of stresses calculated numerically using a finite element method and those calculated according to the HRR solution recommended for the predominantly plane strain conditions. The author of this paper suggests that the use of the parameter Q^{pso} is a good approach because it shows the difference between the actual distribution of stresses responsible for the crack opening and the distribution determined according to a theoretical solution for a case of the dominance of plane strain. The application of the actual stress state seems suitable because, under laboratory conditions, fracture toughness is estimated assuming the presence of the predominantly plane strain conditions, which should be ensured by appropriate geometric dimensions of the structural elements, i.e. the specimen width, the crack length (or the length of the uncracked ligament) and the specimen thickness.

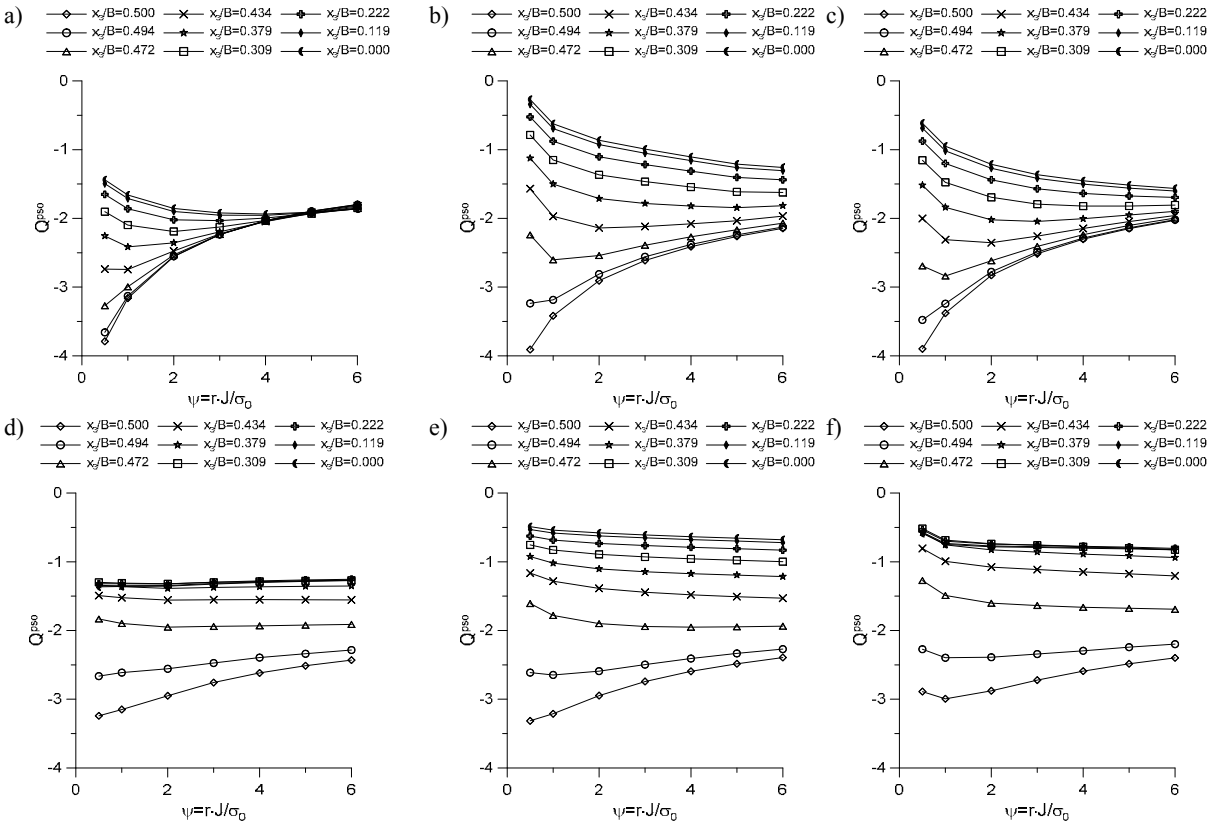

Fig.9. Distributions of the values of the parameter Q^{pso} along the crack front for seven normalized distances, obtained for the specimens under tension at $a/W=0.70$, $W=40mm$, $n=5$, $\sigma_0=315$MPa, $P/P_0=1.20$: a) CC(T) $B=2mm$; b) DEN(T) $B=2mm$; c) SEN(T) $B=2mm$; d) CC(T) $B=40mm$; e) DEN(T) $B=40mm$; f) SEN(T) $B=40mm$.

Figure 9 shows the distribution of the values of the parameter Q^{pso} around the crack front for the CC(T), DEN(T) and SEN(T) specimens considered in this paper. The results are given for the particular layers across the specimen thickness. As can be noticed, the parameter Q^{pso} reaches the lowest values near

the crack tip. The closer to the specimen axis ($x_3/B=0$), the higher the value of the parameter Q^{pso}. For specimens with a small thickness ($B/W=0.05$), the value of the parameter Q^{pso} decreases in the layers located closer to the specimen axis with an increase in the distance from the crack tip (Figs 9a-c). The closer to the specimen edge ($x_3/B=0.5$), the lower the value of the parameter Q^{pso} in the particular layers. For the layers located close to the specimen edge, the values of the parameter Q^{pso} increase with an increase in the distance from the crack tip (Figs 9a-c). For the analyzed range of distances from the crack tip, the lowest values of the parameter Q^{pso} are observed for the CC(T) specimen, while the highest for the DEN(T) specimen. In the case of specimens with a larger thickness ($B/W=1$), we can see that the value of the parameter Q^{pso} is nearly constant regardless of the distance from the crack tip for the layers located in the range of normalized coordinates from $x_3/B=0$ (the specimen axis) to $x_3/B=0.472$ for the CC(T) specimen and to $x_3/B=0.379$ for the DEN(T) and SEN(T) specimens (Figs 9d-f). In the other layers, the values of the parameter Q^{pso} change almost linearly with an increasing distance from the crack tip, but for the layers located very close to the specimen edge ($x_3/B=0.5$), the value of the parameter Q^{pso} increases with an increasing distance from the crack tip (Figs 9d-f). A smaller value of the parameter Q^{pso} for the layers located close to the edge is not surprising because near the edge we should expect a stress state similar to the state with the dominance of plane stress. Along the specimen axis, the state is expected to be similar to that with the dominance of plane strain.

Figure 10 compares the values of the parameters Q^{pso} and Q^{*} averaged across the thickness, designated as Q^{pso}_{av} and Q^{*}_{av}. The results were obtained at two distances from the crack tip, $r=1.0 \cdot J/\sigma_0$ and $r=2.0 \cdot J/\sigma_0$, for a whole spectrum of loads. The value of the parameter Q^{pso}_{av} decreases with an increasing external load (expressed by the level of the J-integral). The lowest values of the parameter Q^{pso}_{av} are reported for the CC(T) specimens, while the highest for the DEN(T) specimens (Fig.10a). As can be seen, the differences between the values of the parameter Q^{pso}_{av} for the two analyzed distances from the crack tip are small for all the specimen types considered. In the case of the SEN(T) specimen, the curves $Q^{pso}_{av}=f(J)$ almost coincide for both distances from the crack tip. The $Q^{*}_{av}=f(J)$ curves, however, are slightly different (compare Figs 10b and 10c). Initially, the parameter Q^{*}_{av} decreases with an increasing external load, but then after the curve $Q^{*}_{av}=f(J)$ reaches a minimum, the parameter Q^{*}_{av} increases. The lowest values of the parameter Q^{*}_{av} are observed for the CC(T) specimens, while the highest for the DEN(T) specimens (Figs 10b and 10c, respectively). The further from the crack tip, the higher the value of the parameter Q^{*}_{av} at the same value of the external load.

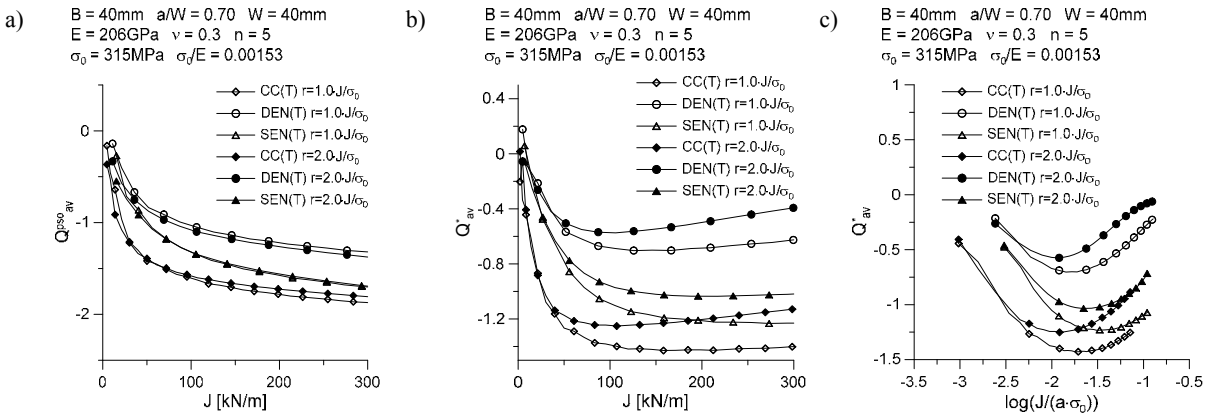

Fig.10. Comparison of the values of the parameters Q^{pso} (a) and Q^{*} (b, c) averaged across the thickness of the CC(T), DEN(T) and SEN(T) specimens at $B=40mm$, $a/W=0.70$, $W=40mm$, $n=5$, $\sigma_0=315$MPa, with the results reported for a whole spectrum of loads.

A comprehensive analysis of the parameters Q^{pso}_{av} and Q^{*}_{av} should also indicate the dependence on the thickness, the crack length and the material constants – see Fig.11. Figures 11a and 11b indicate a clear influence of the thickness on the values of the parameters Q^{pso}_{av} and Q^{*}_{av}. The smaller the thickness, the lower the value of the parameter Q^{pso}_{av}. Specimens with a smaller thickness are characterized by a lower level of geometric constraints (Fig.11a). An increase in the thickness causes an increase in the level of

constraints expressed by the parameter Q^{pso}_{av} (Fig.11a). In the case of the parameter Q^{*}_{av}, an inverse relationship is observed (Fig.11b); the greater the thickness, the lower the value of the parameter Q^{*}_{av}.

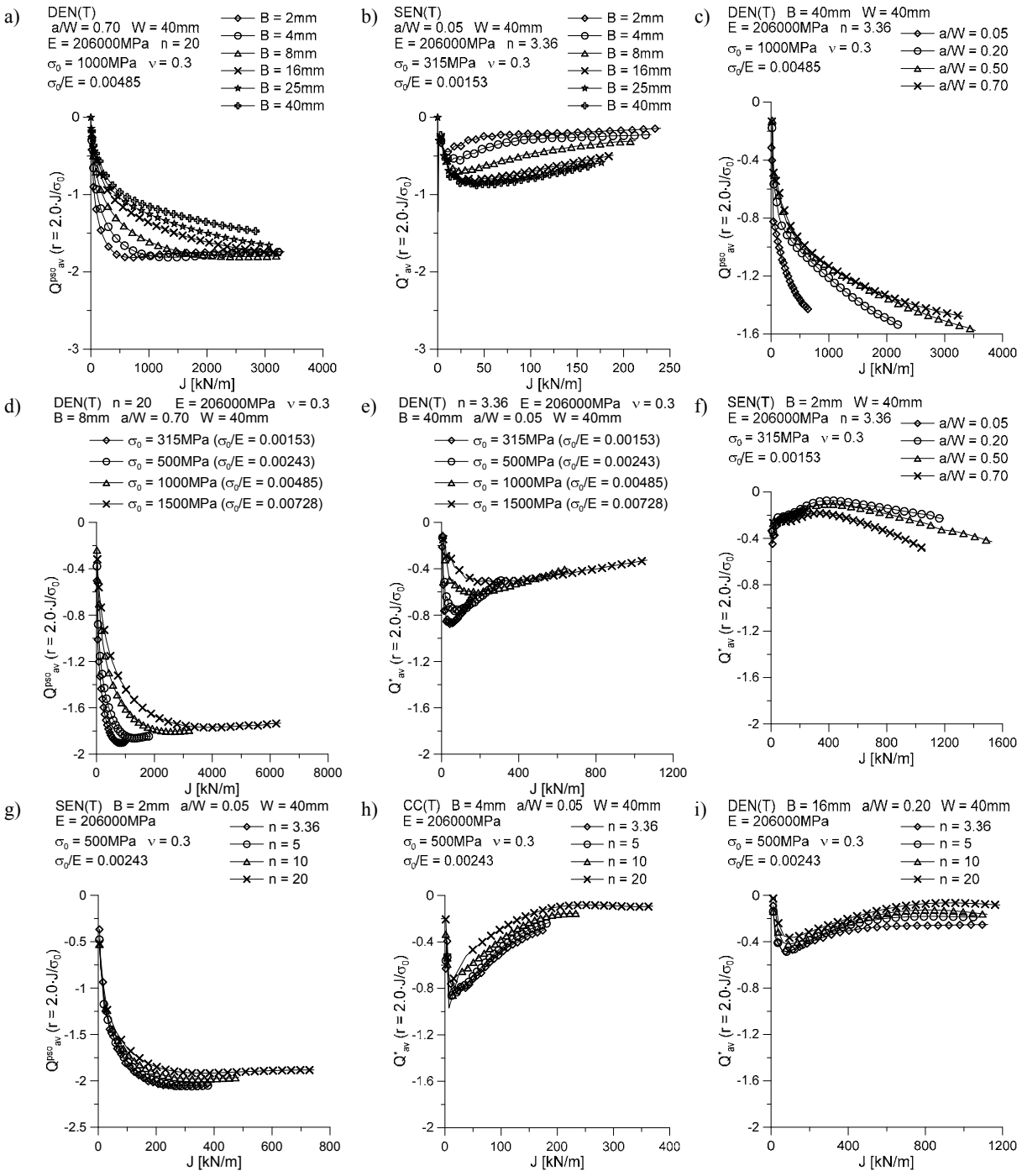

Fig.11. Relationship between the specimen thickness and the values of the parameters Q^{pso}_{av} and Q^{*}_{av} (a and b, respectively). Influence of the relative crack length a/W on the values of the parameters Q^{pso}_{av} and Q^{*}_{av} (c and f, respectively). Changes in the distribution of the curves $Q^{pso}_{av}=f(J)$ and $Q^{*}_{av}=f(J)$ (d and e, respectively) for the specimens differing in the yield strength. Influence of the strain hardening exponent n in the RO law on the values of the parameters Q^{pso}_{av} and Q^{*}_{av} (g and h and I, respectively).

The two parameters, Q^{pso}_{av} and Q^{*}_{av}, are considered to be measures of the constraints dependent on the crack length (Figs 11c and 11f, respectively). The value of the parameter Q^{pso}_{av} is lower when the crack is shorter and the level of constraints is lower (Fig.11c). The parameter can be identified with Q stresses defined by O'Dowd [9, 10]. The two parameters are calculated in the same way both for the predominantly plane strain conditions and for the three-dimensional problems considered in this paper; the reference state is the level of stresses calculated according to the HRR solution for the predominantly plane strain conditions. In the case of the parameter Q^{*}_{av}, the influence of the relative crack length is illustrated in Fig.11f. As can be seen, the longer the crack length, the smaller the value of the parameter Q^{*}_{av}. However, it is important to note that changes in the values of this parameter are directly related to the stress triaxiality coefficient T_z, which is also calculated numerically. Thus, when the parameter Q^{*}_{av} is calculated, the reference distribution of stresses changes for the particular layers across the specimen thickness. From the analysis of the results of the numerical calculations it is clear that the effect of the crack length should be assessed separately for each geometry, taking into account the appropriate material characteristics.

Figures 11d and 11e illustrate the relationships between the yield strength and the parameters Q^{pso}_{av} and Q^{*}_{av}, respectively. The higher the value of the yield strength, the higher the level of the geometric constraints expressed by the value of the parameter Q^{pso}_{av} (Fig.11d). With the value of the J-integral being the same, the value of the parameter Q^{pso}_{av} will be lower for a material characterized by a low yield strength. The curves $Q^{pso}_{av}=f(J)$ plotted for the specimens under analysis are generally similar in shape; the curves $Q^{pso}_{av}=f(J)$ are lowest for the materials with the lowest yield strength (Fig.11d). In the case of the parameter Q^{*}_{av} (Fig.11e), its values are lower when the yield strength and the J-integral are lower. Then, the curves $Q^{*}_{av}=f(J)$ reach a minimum. However, after an increase in the external load (expressed by the value of the J-integral), the value of the parameter Q^{*}_{av} increases differently, according to the yield strength (Fig.11e).

The two parameters, Q^{pso}_{av} and Q^{*}_{av}, are also dependent on the strain hardening exponent in the RO law. The higher the degree of hardening, the lower the level of the geometric constraints expressed by the parameter Q^{pso}_{av} (Fig.11g). The higher the value of the strain hardening exponent in the RO law, the higher the curves $Q^{pso}_{av}=f(J)$ (Fig.11g). The changes in the parameter Q^{pso}_{av} as a function of the J-integral (expressed by the value of the external load) coincide with the changes in Q stresses determined for specimens under predominantly plane strain conditions, which are described in [7]; it is important to note, however, that the analysis presented in this paper refers to 3D geometries. The parameter Q^{pso}_{av} declines gradually with an increasing external load; for certain configurations of geometry and material, it approaches a state of saturation (Fig.11g). This paper does not contain all the results obtained. The greatest influence of the strain hardening exponent on the distribution of the curves $Q^{pso}_{av}=f(J)$ was reported for the CC(T) specimens, while the smallest for the SEN(T) specimens.

Figures 11h and 11i show changes in the parameter Q^{*}_{av} as a function of the J-integral for specimens with different degrees of material hardening. The higher the degree of hardening, the lower the curves $Q^{*}_{av}=f(J)$. The changes in the values of the parameter Q^{*}_{av} as a function of the J-integral are not uniform; they are dependent on the configuration of the specimen geometry and material. The values of the parameter Q^{*}_{av} obtained for two specimens with the same geometry and yield strength, characterized by extreme values of the strain hardening exponent n in the RO law ($n=3.36$ and $n=20$) differ by about 20%. The lower the degree of hardening, the higher the values of the parameter Q^{*}_{av} at the same value of the J-integral.

5. Conclusions

This paper has briefly analyzed selected measures of the geometric constraints for cracked plates under tension; however, further research in this area is essential. From the author's experience it is evident that determining the relationship between the measures of the constraints, the element geometry and its material characteristics requires considering each geometry separately (see e.g. [7]). This paper has described problems related to these constraints and methods of their assessment; however, creating a complete catalogue of numerical solutions will allow us to fully analyze the different aspects of the definitions of the material, the crack length, the specimen thickness and the variations of these parameters.

The following are the major conclusions drawn from the study of the measures of the geometric constraints determined for certain 3D geometries subjected to tension:

- the distance from the crack tip and the location of the layer across the specimen thickness have a substantial effect on all the measures of geometric constraints considered in this paper for 3D problems;
- the averaged values of the stress triaxiality parameters, $(\sigma_m/\sigma_0)_{av}$, $(\sigma_m/\sigma_{eff})_{av}$ and $(T_z)_{av}$, decrease with an increase in the external load;
- the lowest values of the averaged stress triaxiality parameters, i.e., $(\sigma_m/\sigma_0)_{av}$, $(\sigma_m/\sigma_{eff})_{av}$ and $(T_z)_{av}$, were reported for the CC(T) specimens, while the highest were obtained for the DEN(T) specimens; for the cases studied, the differences between the curves $(\sigma_m/\sigma_0)_{av}=f(J)$, $(\sigma_m/\sigma_{eff})_{av}=f(J)$ and $(T_z)_{av}=f(J)$ were not large;
- the stress triaxiality parameters, i.e., $(\sigma_m/\sigma_0)_{av}$, $(\sigma_m/\sigma_{eff})_{av}$ and $(T_z)_{av}$, are practically independent of the relative crack length, as suggested in [7];
- the material constants, i.e., the yield strength and the exponent in the RO law, affect the parameters $(\sigma_m/\sigma_0)_{av}$, $(\sigma_m/\sigma_{eff})_{av}$ and $(T_z)_{av}$; the influence of the yield strength is very clear, but the strain hardening exponent is responsible for a difference of about 15% between the values of the same stress triaxiality parameters for a material undergoing considerable strain hardening ($n=3.36$) and a material exhibiting poor strain hardening ($n=20$);
- the specimen thickness has a considerable effect on the averaged measures of the geometric constraints discussed in this paper, i.e., stress triaxiality parameters – $(\sigma_m/\sigma_0)_{av}$, $(\sigma_m/\sigma_{eff})_{av}$ and $(T_z)_{av}$ – as well as measures of the in-plane constraints [7] – $Q^{pso}{}_{av}$ and $Q^{*}{}_{av}$;
- the averaged values of the measures of geometric constraints in the form of the parameters $Q^{pso}{}_{av}$ and $Q^{*}{}_{av}$ are greatly dependent on the relative crack length, the strain hardening exponent and the yield strength; the relationships between the measures of the constraints and the different factors should be studied separately for each geometry, as shown in [7], using the example of Q stresses defined by O'Dowd [9, 10].

In the near future, the author of this paper intends to develop a program code with a built-in library of numerical solutions, which will contain all the FEM-based calculation results concerning the assessment of elastic-plastic parameters of fracture mechanics, which can be considered as measures of geometric constraints. The library of numerical solutions could be used to handle engineering problems, for example, the determination of the state of stresses around the crack front in three-dimensional structural elements or the determination of fracture toughness or tensile strength of structural elements using failure assessment diagrams (FADs) or the crack driving force (CDF) technique [16].

Acknowledgements

The research reported herein was supported by a grant from the Faculty of Mechatronics and Machine Design at Kielce University of Technology (project No. 01.0.09.00/2.01.01.01.0027 MNSP.MKTM.17.002).

Nomenclature

a	–	crack length
a/W	–	relative crack length
B	–	specimen thickness
b	–	uncracked ligament of the specimen ($b=W-a$)
CC(T)	–	center cracked plate in tension
CDF	–	Crack Driving Force Diagram
DEN(T)	–	double edge notched cracked plate in tension
E	–	Young's modulus
ES_{max}	–	size of the largest FE

ES_{min} – size of the smallest FE
$f(t)$ – time function
FAD – Failure Assessment Diagram
FE – Finite Element
FEM – Finite Element Method
FITNET – European FITness-for-service NETwork
HMH – Huber-Misses-Hencky hypothesis
HRR – Hutchinson-Rice-Rosengren
i, j – components of the stress tensor
$I_n(n, pso)$ – quantity dependent on the material through the exponent n, and the method of loading, calculated for the plane strain state
$I_n(n, T_z)$ – quantity dependent on the material through the exponent n, the T_z parameter, the method of loading and the specimen thickness
J – J – integral
J_{far} – J – integral calculated numerically using far-field integration contour
n – strain hardening exponent in the Ramberg-Osgood relationship
Q – Q - stress defined by O'Dowd and Shih
Q^* – the in-plane constraints parameter defined by Graba and Neimitz (the differences between numerical stresses and Guo solution)
Q^*_{av} – average across the specimen thickness value of the Q^* parameter
Q^{pso} – the in-plane constraints parameter defined as the differences between numerical stresses and HRR solution for plane strain state
Q^{pso}_{av} – average across the specimen thickness value of the Q^{Ppso} parameter
P – external load
P_0 – limit load
r, θ, z – coordinates of the polar coordinate system hooked on crack tip
r_w – radius of the arc in crack tip
SEN(T) – single edge notched cracked plate in tension
T_z – stress triaxiality coefficient defined by Guo Wanlin
v_{LL} – load line displacement
W – width of the specimen
x_1, x_2, x_3 – Cartesian coordinates: x_1, x_2 - in the crack plane, x_3 - in the thickness direction
x_3/B – normalized coordinate in the thickness direction ($x_3/B=0$ – center of the specimen, $x_3/B=0.5$ – free surface of the specimen)
α – constant in the Ramberg-Osgood relationship
ν – Poisson's ratio
ψ – normalized distance from the crack tip, calculated as $\psi=r\cdot J/\sigma_0$
$(\sigma_m/\sigma_0)_{av}$ – average across the specimen thickness value of the σ_m/σ_0 ratio (parameter)
$(\sigma_m/\sigma_{eff})_{av}$ – average across the specimen thickness value of the σ_m/σ_{eff} ratio (parameter)
ε_0 – strain corresponding to the yield stress ($\varepsilon_0=\sigma_0/E$)
σ_0 – yield stress
$\sigma_{11}, \sigma_{22}, \sigma_{33},$ – normal components of the stress tensor
σ_{22_FEM} – numerical value of crack opening stresses
σ_{22_GUO} – the value of crack opening stresses resulting from the Guo solution
σ_{22_pso} – the value of crack opening stresses resulting from the plane strain state solution
σ_{eff} – effective stresses calculated according to the HMH hypothesis
σ_{ij} – stress tensor defined for 3D issues
σ_{ij_pso} – stress tensor defined for plane strain state
σ_m – normal stresses
$(T_z)_{av}$ – average across the specimen thickness value of the T_z parameter
$\widetilde{\sigma_{ij}}(\theta, n, T_z)$ – functions dependent on the material through the exponent n, the angle θ and T_z parameter
$\widetilde{\sigma_{ij}}(\theta, n, pso)$ – functions dependent on the material through the exponent n, the angle θ, calculated for plane strain state
2D – two dimensional
3D – three dimensional

References

[1] Hutchinson J.W. (1968): *Singular Behavior at End of Tensile Crack in Hardening Material.* – Journal of the Mechanics and Physics of Solids, vol.16, No.1, pp.13-31.

[2] Rice J.R. and Rosengren G.F. (1968): *Plane strain deformation near crack tip in power-law hardening material.* – Journal of the Mechanics and Physics of Solids, vol.16, No.1, pp.1-12.

[3] Guo W. (1993a): *Elastoplastic three dimensional crack border field – I. Singular structure of the field.* – Engineering Fracture Mechanics, vol.46, No.1, pp.93-104.

[4] Guo W. (1993b): *Elastoplastic three dimensional crack border field – II. Asymptotic solution for the field.* – Engineering Fracture Mechanics, vol.46, No.1, pp.105-113.

[5] Guo W. (1995), *Elastoplastic three dimensional crack border field – III. Fracture parameters.* – Engineering Fracture Mechanics, vol.51, No.1, pp.51-71.

[6] Graba M. (2007): *The description of the stress fields for elastic-plastic materials – 3D issues.* – Proceeding of the XI National Fracture Mechanics Conference, Kielce - Cedzyna, 8-12.09.2007., printed abstract - pp.33-34, electronic version of the article - 28 pages (in Polish).

[7] Graba M. (2009): *Numerical analysis of the mechanical fields near the crack tip in the elastic-plastic materials. 3D problems.* – PhD dissertation, Kielce University of Technology - Faculty of Mechatronics and Machine Building, 387 pages, Kielce 2009 (in Polish).

[8] Neimitz A. and Graba M. (2008): *Analytical-numerical Hybrid Method to Determine the Stress Field in Front of the Crack in 3D Elastic-plastic Structural Elements.* – Proceeding of the XVII European Conference of Fracture (ECF), Brno – Czech Republic, 1-4.09-2008., electronic version of the article on CD, abstract - book of abstracts p.85.

[9] O'Dowd N.P. and Shih C.F. (1991): *Family of crack-tip fields characterized by a triaxiality parameter – I. Structure of fields.* – J. Mech. Phys. Solids, vol.39, No.8, pp.989-1015.

[10] O'Dowd N.P. and Shih C.F. (1992): *Family of crack-tip fields characterized by a triaxiality parameter – II. Fracture applications.* – J. Mech. Phys. Solids, vol.40, No.5, pp.939-963.

[11] Graba M. (2012), *Proposal of the three-parametric fracture criterion for brittle materials.* – The Mechanical Review, No.2, pp.24-31 (in Polish).

[12] Neimitz A., Dzioba I., Molasy R. and Graba M. (2004): *The influence of the constraints on fracture toughness for brittle materials.* – Proceeding of the XX Symposium of the Fatigue and Fracture Mechanics, Bydgoszcz-Pieczyska, 27-30.04.2004r., pp.265-272 (in Polish).

[13] Neimitz A. and Gałkiewicz J. (2006): *Fracture toughness of structural components: influence of constraint.* – International Journal of Pressure Vessels and Piping, vol.83, pp.42-54.

[14] Graba M. (2008): *The influence of material properties on the Q-stress value near the crack tip for elastic-plastic materials*. – Journal of Theoretical and Applied Mechanics, vol.46, No.2, pp.269-289.

[15] Graba M. (2011): *The influence of material properties and crack length on the Q-stress value near the crack tip for elastic-plastic materials for centrally cracked plate in tension.* – Journal of Theoretical and Applied Mechanics, vol.50, No.1, pp.23-46.

[16] Neimitz A., Dzioba I., Graba M. and Okrajni J. (2008): *The assessment of the strength and safety of the operation high temperature components containing crack.* – Kielce University of Technology Publishing House, Kielce, 428 pages (in Polish).

[17] McClintock F.A. (1968): *A criterion for ductile fracture by growth of holes.* – Journal of Applied Mechanics, vol.4, pp.363-371.

[18] Rice J.R. and Tracey D.M. (1971): *On the ductile enlargement of voids in triaxial stress fields.* – Journal of the Mechanics and Physics of Solids, vol.17, pp.201-217.

[19] Henry B.S., Luxmoore A.R. and Sumpter J.D.G. (1996): *Elastic-plastic fracture mechanics assessment of low constraint aluminum test specimens.* – International Journal of Fracture, No.81, pp.217-234.

[20] Kim Y., Chao Y.J. and Zhu X.K. (2003): *Effect of specimen size and crack depth on 3D crack-front constraint for SENB specimens.* – International Journal of Solids and Structures, vol.40, pp.6267-6284.

[21] Kim Y., Zhu X.K. and Chao Y.J. (2001): *Quantification of constraint on elastic-plastic 3D crack front by the J-A_2 three-term solution.* – Engineering Fracture Mechanics, vol.68, pp.895-914.

[22] FITNET (2006): *FITNET Report, (European Fitness-for-service Network).* – Edited by M. Kocak, S. Webster, J.J. Janosch, R.A. Ainsworth, R. Koers, Contract No. G1RT-CT-2001-05071, 2006.

[23] Sumpter J.D.G. and Forbes A.T. (1992), *Constraint Based Analysis of Shallow Cracks in Mild Steel.* – TWI/EWI/IS International Conference on Shallow Crack Fracture Mechanics Test and Application, M.G. Dawes, Ed., Cambridge, UK, paper 7.

[24] ADINA 8.8 (2011a): *ADINA: User Interface Command Reference Manual – Volume I: ADINA Solids & Structures Model Definition.* – Report ARD 11-2, ADINA R&D, Inc., 2011.

[25] ADINA 8.8 (2011b), *ADINA: Theory and Modeling Guide – Volume I: ADINA Solids & Structures.* – Report ARD 11-8, ADINA R&D, Inc., 2011.

[26] Graba M. (2013): *Numerical verification of the limit load solutions for single edge notch specimen in tension.* – Archives of Civil and Mechanical Engineering, vol.13, No.1, pp.45-56.

[27] Graba M. (2013): *Extension of the concept of limit loads for 3D cases for a centrally cracked plate in tension* – Journal of Theoretical and applied mechanics, vol.51, No.2, pp.349-362.

Received: July 24, 2017

Revised: September 13, 2017